ARKIV FÖR FYSIK Band 15 nr 1

Communicated 3 December 1958 by Erik Hulthén and Kai Siegbahn

# Systematic study of electron binding energies of some fourth and sixth period elements by means of the photo electron method

By Evelyn Sokolowski

With 29 figures in the text

ABSTRACT

A new precision method of measuring electron binding energies is used in a systematic study of $K$ energies in the fourth and $L$ energies in the sixth period of the periodic table. The results are compared to those obtained by the conventional X-ray absorption method. Discrepancies are observed in some cases, which motivates a reconsideration of the fundamental processes involved in the two methods. The use of infinitely thick sources in $\beta$-spectroscopy is demonstrated.

## I. Introduction

The concept of electron binding energy is as old as the Bohr model of the atom. In terms of this model the definition of binding energy seems obvious: it should be the energy required to lift an electron from its original shell to infinity. The experimental method usually employed to study electron binding has been that of X-ray absorption [1]. The absorption edge is due to the excitation of an atom from its—unambiguous—ground state to a state where an "inner" electron has been lifted to the empty region above the Fermi level. Thus, the structure of this region will be mirrored in the absorption edge to the extent that this is allowed by selection rules. This fact shows that it is difficult to decide on an adequate definition of electron binding energy in terms of X-ray absorption edges. The definition that seemed obvious in view of the Bohr model is impracticable from the viewpoint of the X-ray spectroscopist, since the point on an absorption curve, corresponding to the removal of an electron to infinity with zero kinetic energy, is impossible to identify. As shown below, this energy can be uniquely determined in the photo electron spectrum of a solid, but even so, it is not suited to define the binding energy, since it includes the work function of the crystal, which in turn is sensitive to the particular experimental conditions.

In X-ray spectroscopy one has generally agreed to define the binding energy of an inner electron shell as the energy associated with an electron transition from that

inner shell to the lowest unoccupied level in the conduction band. This definition was related to experiment by Richtmyer, Barnens and Ramberg [2], who showed that, under the assumption of a constant density of states around the first unoccupied level, the absorption edge should follow an arc tan function, the inflection point of which should correspond to transitions to the lowest unoccupied state in the conduction band. The first inflection point of the absorption edge has thus become the empirical criterion of binding energy. The assumption of a constant level density has of course limited validity and the deviation of experimental absorption curves from arctan functions is often pronounced. Further, the theory of Richtmyer, Barnes and Ramberg does not take into account selection rules, which might altogether inhibit transitions to the lowest unoccupied state. These facts together lead to the conclusion that the possible systematic errors inherent in the X-ray method are primarily to be sought in the physical picture on which the interpretation of the data is based. In some cases the experimental uncertainties must also be taken into consideration. They will be discussed in greater detail below.

The difficulties in interpreting X-ray absorption curves have induced several investigators to attempt different ways of studying electron binding. Some early attempts in this direction have already been cited in reference [3]. For a long time the accuracies achieved were such that the methods could not compete favourably with the standard X-ray methods. In reference [3] we described the successful development of an alternative method, based on the magnetic analysis of X-ray photo electrons. The improvement of the results was mainly due to refined techniques for analyzing the electron spectrum. The preliminary experiments reported in [3] have now been extended to a more systematic study of electron binding energies. It was hoped that a comparison between the results thus obtained and the old X-ray values should throw light on both methods.

## II. Principles of the present method

Figure 1 is a schematic drawing of the experimental arrangement, a detailed description of which has already been given in [3] and [4]. Since in the present method the out-going electron remains an integral part of the system studied, all electrostatic potentials must be well defined and we are restricted to studying metallic or semiconducting substances. It is essential that the electron source is well grounded to the copper tank of the spectrometer. Figure 2 shows a schematic diagram of the upper energy levels of two metals in contact. The Fermi surface corresponds to the boundary between the region of filled levels (valence band) and the empty region (conduction band). Since the levels in the conduction band are much narrower than the inner electron levels we get, according to the usual X-ray spectroscopic definition, that the binding energy of an inner level in a metal is the energy of a transition from that level to the Fermi surface. If the inner electron is removed from the crystal it must, in addition, overcome the work function $\phi$. The vacuum level is the final state of an electron, which has been removed from the crystal with zero kinetic energy. If the excitation energy for the photo electron, $h\nu$, exceeds the binding energy plus the work function, the electron may leave the crystal with a certain kinetic energy according to the expression

$$h\nu - \text{K.E.} = \text{B.E.} + \phi. \qquad (1)$$

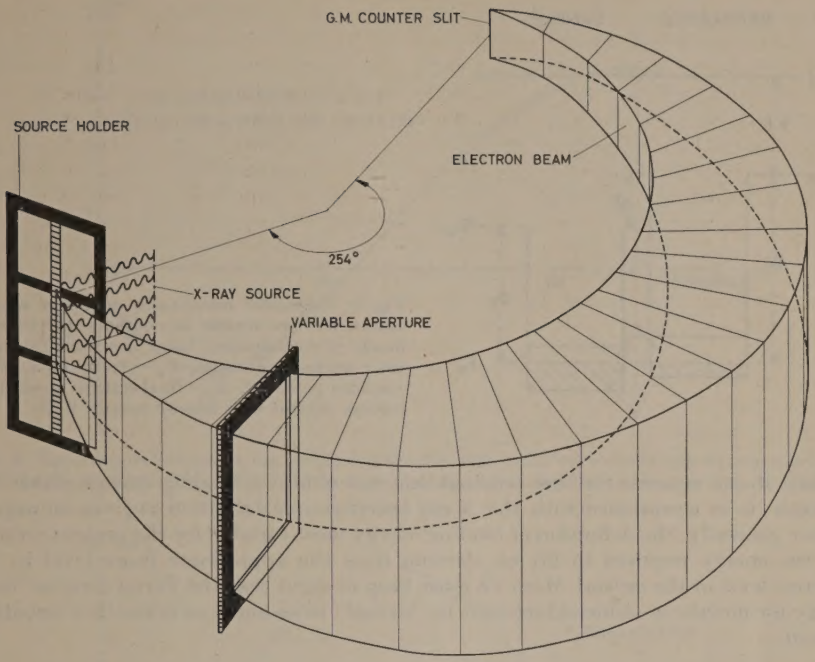



Fig. 1. Schematic view of experimental arrangement. The sources are evaporated onto 15 $\mu$ Al strips, with calibration samples on two of the sections of the source holder. The three sections can be slid into the X-ray beam successively.

In the present case, the quantities to the left are known from experiment, the former from X-ray emission data and the latter from the magnetic analysis of the electron momenta.

It is a well-known fact that for two crystals in contact, the equilibrium condition is that the Fermi levels coincide [5]. For crystals with good electronic conductivity equilibrium is established instantaneously. The vacuum levels then become separated by the difference in work function, or contact potential, $\Delta\phi$, of the two crystals. In figure 2, the right hand side represents the sample under investigation, while the left hand side, denoted by "reference", symbolizes the spectrometer. The figure makes it clear that the measured energy of the photo electron will depend on what vacuum potential the electron is sensing during the magnetic analysis. From the geometry of the experiment it seems probable that the spectrometer potential should be the dominating already within a very short distance of the source. This was tested by placing a copper mesh just in front of the sample [4], thus bringing the spectrometer vacuum potential very close to the source. No change in the measured energy of a line could be detected, proving that the electron is accelerated (or decelerated) to the spectrometer potential and "forgets" its origin before the magnetic analysis sets in. From the above it is clear that the quantity $\phi$ in equation 1 should be the work function of the spectrometer material and the same for all measurements.

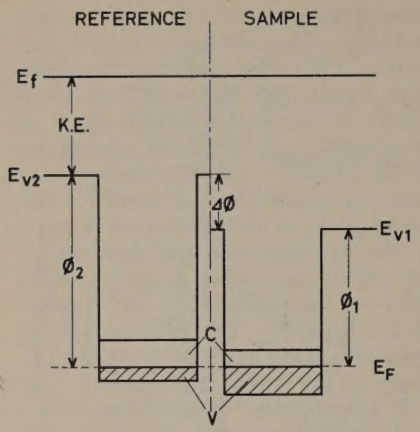



Fig. 2. Schematic relationship of upper energy bands for two metals in contact. $V$ = valence band; $C$ = conduction band; $\phi$ = work function; $\Delta\phi$ = contact potential; $E_F$ = Fermi level; $E_v$ = vacuum potential; $E_f$ = final state of an electron leaving crystal with kinetic energy K.E.

Thus, if one corrects for this constant one can obtain a binding energy which, for metals, is in accordance with the X-ray spectroscopic definition as given on page 1. More generally, the definition of binding energy most suitable for the present method is the energy required to lift an electron from the appropriate inner level to the Fermi level of the crystal. Here we must keep in mind that the Fermi level is "real" only for metals; in semiconductors it is "virtual" in as much as it lies in a forbidden band.

## III. Experimental conditions

### A. *Magnetic field control*

A fundamental requirement for accurate energy determinations is the precise control of the magnetic field. For an iron-free spectrometer the problem of determining the spectrometer field reduces to a measurement of the coil current, or if, as in the present case, calibration lines are used, a measurement of some quantity proportional to the current. This is performed with the aid of an AEG compensator as described in ref. [6]. Since we are not interested in absolute current measurements the requirements on the compensator components are less stringent than would otherwise be the case. The Weston standard cell, for instance, need only be kept constant during the course of a measurement.

It is clear that each calibration constant pertains only to a certain field distribution with respect to the source-, aperture- and detector positions. This makes it necessary to keep the temperature of the spectrometer coils constant with respect to the vacuum tank. The temperature equilibrium conditions have been studied by means of thermocouples and have been reported in ref. [4].

An uncertainty in the total magnetic field is due to fields other than those produced by the spectrometer coils. The most important stray component is the earth field, but magnets from other laboratories were also found to contribute significantly. It is safe to assume that all sources of stray fields are far enough away from the spectrometer to give rise to homogeneous fields over the spectrometer volume. To

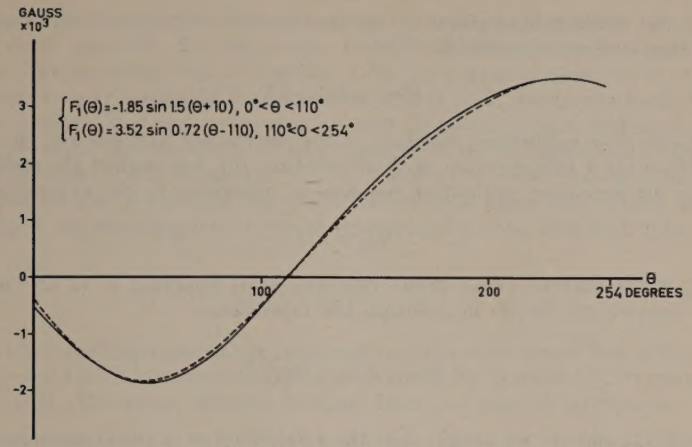



Fig. 3. Experimental shape of the residual magnetic field (solid curve) and sine approximation $F_1(\theta)$ (dashed curve). The field is taken to be positive when parallel to the spectrometer field.

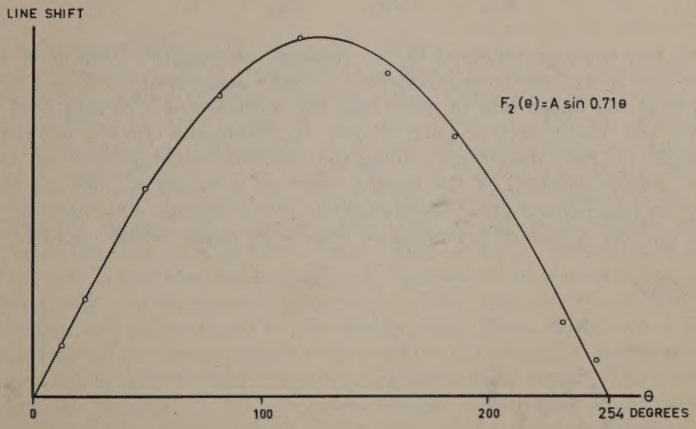



Fig. 4. Weight function $F_2(\theta)$ for the residual magnetic field. The circles correspond to the experimental points.

compensate for stray fields the spectrometer is equipped with three perpendicular sets of Helmholtz coils. It was found in ref. [6] that if the stray fields are balanced out at the center of the spectrometer, the Helmholtz coils leave a periodic field along the electron trajectory with a maximum value of $3.5 \times 10^{-3}$ gauss. As shown in fig. 3, the residual field can be well represented by the two sine functions

$$F_1(\theta) = -1.85 \sin 1.5(\theta + 10), \quad 0° < \theta < 110°,$$

$$F_1(\theta) = 3.52 \sin 0.72(\theta - 110), \quad 110° < \theta < 254°.$$

If $\Delta B$ is the residual field and $I$ is the spectrometer current we may write for any electron line with momentum $B\varrho$ that

$$B\varrho = \varkappa I + \varrho \Delta B. \tag{2}$$

Here $\varkappa$ is the true calibration constant of the instrument and $\varrho$ is the spectrometer radius. If we use a reference line with momentum $B\varrho_1$ but neglect the residual field, we obtain an erroneous calibration constant $\varkappa'$ according to the expression

$$B\varrho_1 = \varkappa' I_1, \tag{3}$$

where $I_1$ is the current value of the reference line. Applying $\varkappa'$ to an "unknown" electron line we get for *its* momentum the false value

$$B\varrho_2' = \varkappa' I_2 = B\varrho_1 \frac{I_2}{I_1}. \tag{4}$$

Then from (2) and (4) we obtain that the relative error in the momentum of line 2 due to the neglect of the residual field is

$$\frac{\Delta B\varrho_2}{B\varrho_2} = \frac{B\varrho_2 - B\varrho_2'}{B\varrho_2} = \frac{\varrho \Delta B}{B\varrho_2}\left(1 - \frac{I_2}{I_1}\right). \tag{5}$$

With the low energies involved in the present investigation this error cannot be neglected and it was therefore of interest to make an accurate estimate of the mean residual field. We must bear in mind that the influence of a certain field is not the same over the whole electron path. Hence, to obtain the *effective* residual field we must weight the field distribution along the electron trajectory with an appropriate function. The calculation of the weight function is rather tedious for the present geometry and an experimental determination of the function was therefore preferred. For this purpose a pair of perturbation coils were made, which could be slid along

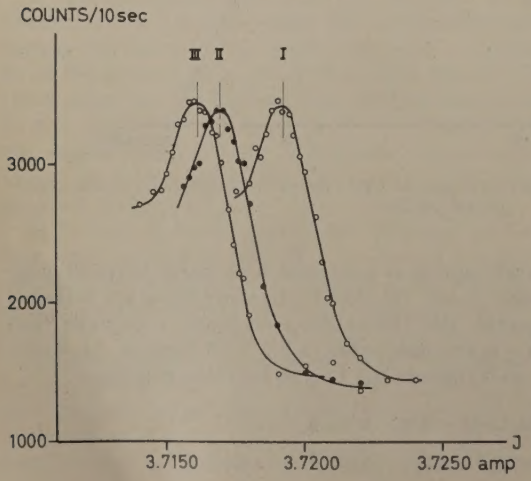



Fig. 5. Three recordings of the A6 Auger line of Cu used for the determination of the function $F_2(\theta)$. Recording I was taken without the perturbation coils, II with the perturbation coils at 190°, and III with the coils at 115°.

the optical axis of the spectrometer, one coil above and the other below the vacuum tank. The space available did not permit ideal Helmholtz dimensions for the coil system, but the dimensions used (coil radius = 7.5 cm, distance between coils = 12 cm) were expected to give a roughly homogeneous central field, decreasing fairly rapidly outside the system. The coils were wound with 20 turns in each and used with a current of 100 mA. The spectrometer was focussed on the strongest line in the *KLL* Auger spectrum of Cu (fig. 5; see also ref. 7), the shift of which was then measured as a function of the position of the perturbation coils along the optical axis. As shown in fig. 4 the resulting curve can be represented by the first half cylce of the function

$$E_2(\theta) = A \sin \frac{\pi}{\theta_0} \cdot \theta, \tag{6}$$

where $\theta_0$ is the focussing angle of the spectrometer. The same result has been derived theoretically for a 180° homogenous field spectrometer by Hartree [8]. In the present case $\pi/\theta_0 = 0.71$. The mean effective residual field can now be written as

$$\Delta B = \frac{\int_0^{254^\circ} F_1(\theta) \sin 0.71\,\theta\, d\theta}{\int_0^{254^\circ} \sin 0.71\,\theta\, d\theta} \cdot \tag{7}$$

Evaluating the integral gives $\Delta B = 7.0 \times 10^{-4}$ gauss.

The field distribution $F_1(\theta)$ is valid when the magnetic field at the center of the spectrometer is zero. This condition was maintained throughout the measurements. Field determinations in the region of $10^{-4}$ gauss pose a difficult problem, the ordinary methods based on fluxmeters or proton resonance being too insensitive. As in ref. [6], a magnetometer of the type 1.100 from Institut Dr. Förster, having a maximum sensitivity of $10^{-5}$ gauss, was used in the present experiments. The probe of this instrument consists of a special alloy core of high permeability which is driven beyond saturation by a high frequency signal. A signal induced in a pick-up coil around the core is analyzed electronically. If no steady field is present the induced signal contains only odd harmonics; with such a field, even harmonics will occur, whose amplitudes are proportional to the steady field. From the above it is clear that the calibration of the instrument is very sensitive to a change in permeability. It was found that ageing affected the instrument probe to some extent. The sensitivity decreased, and the response of the instrument became asymmetric about zero when the probe had been exposed to a field of the order of a few gauss. In spite of the changes in characteristics the instrument could still be used as a zero indicator, the true zero position being that where the instrument reading remained the same when the probe was turned 180°. However, the absolute reading of the instrument could no longer be completely trusted. For this reason it was preferred to completely balance out the magnetic field in the center of the spectrometer instead of adjusting it to some value different from zero that would have reduced the effective residual field along the electron path.

### B. *Energy calibration*

For absolute energy determinations with a $\beta$-spectrometer Siegbahn [9] has described a "self-consistent" method which makes use of the known energy difference

between two electron lines. This method has been applied to the conversion electrons of ThB in ref. [6], where a detailed discussion of the errors involved is given. It is clear that, to achieve high accuracy with the "self-consistent" method of calibration, one should strive for as great a momentum ratio as possible between the two lines to be measured. On the other hand, if the lines differ widely in energy, new sources of error may appear. Thus, the two lines may differ considerably in shape due to the difference in instrument resolution at the two energy settings, making it difficult to identify corresponding points on the lines. Also, equation 5 shows that relative errors due to incompletely balanced stray fields become more serious the greater the momentum ratio. In general one may thus expect the "self-consistent" calibration method to be impaired by greater errors than would be a calibration employing a line of known momentum in the vicinity of the unknown line. For this reason absolute energy determinations were made only for a few electron lines, which were then in turn used as calibration lines for the other, close-lying, lines measured in this investigation. The possible greater errors in the basic absolute calibration then enter into the subsequent relative energy measurements as systematic errors and do not obliterate the general trend of the binding energy as a function of $Z$.

The elementary constants on which all the numerical values are based are those given by DuMond and Cohen in 1953 [10]. This set of constants was chosen in order to provide consistency with the tables used for the conversion from momentum to energy [11], as well as with ref. [6], on which one of the absolute calibrations is founded. For the basic reference line was chosen the photo line, resulting from conversion of Mo $K\alpha_1$ radiation in the $K$ shell of Cu, henceforth denoted by Cu $K$(Mo $K\alpha_1$). The momentum of this line was measured against the "$F$" conversion line of ThB in ref. [3] and found to be 312.070[1] gauss-cm. However, this value has not been corrected for the effective residual field. The current values for the Cu $K$(Mo $K\alpha_1$)- and the $F$ lines being roughly 4.09 and 18.19 amps respectively, this correction becomes, according to (5)

$$\Delta B\varrho = +1.6 \times 10^{-2} \text{ gauss-cm.}$$

In some of the measurements it proved more convenient to use the strongest line in the $KLL$ Auger spectrum of Cu, denoted by A6, as a reference. The momentum of this line had been related to that of Cu $K$(Mo $K\alpha_1$) by a series of many measurements, so that the additional error involved in this step is small.

Two independent absolute determinations of the Cu $K$(Mo $K\alpha_1$) momentum have been carried out by Nordling [12]. The $B\varrho$ values of the reference lines, resulting from the different determinations, are listed in table 1. All the values have been corrected for the residual magnetic field.

Experimentally, the calibrations were carried out in essentially the same way as in ref. [4]. The source holder consisted of three sections, which could be slid into the X-ray beam successively, two of the sections holding the calibration substance and the third the sample under investigation. Thorough tests of this arrangement had shown that the source position could usually be well reproduced with the three sections. If there was a slight shift between lines from the three sections, corresponding to the same energy, this shift was linear, and hence, by mounting the calibration

[1] In ref. [3] this value was given with only five figures. The sixth figure was found to be justified after a renewed analysis of the data.

*Table 1.*

| Line | $B\varrho$ (gauss-cm) | Source | Mean |
|---|---|---|---|
| Cu $K$(Mo $K\alpha_1$) | 312.086 ± 0.017 | Calibr. against $F$ line | 312.092 ± 0.010 |
| | 312.096 ± 0.025 | Ref. [12] | |
| | 312.095 ± 0.020 | Ref. [12] | |
| A6 | 283.794 ± 0.018 | Measured against $F$ line via Cu $K$(Mo $K\alpha_1$) | 283.798 ± 0.010 |
| | 283.801 ± 0.017 | Ref. [12] | |

The errors given here are the mean errors, in contrast to ref. [3], where the maximum errors were given.

substance on two of the sections, it was possible to obtain the corresponding current value for the geometry of the third section by interpolation.

### C. *Line shape*

Elementary quantum mechanical considerations [13] lead to the result that the probability of transition to an excited atomic level follows a Hoyt distribution:

$$I(E) = \frac{A\,\Gamma^2}{\Gamma^2 + E^2}, \tag{8}$$

where $2\Gamma$ is the width at half maximum. The energy giving maximum amplitude we speak of as the energy of the level in question. The Hoyt distribution is characterized by the fact that if we fold it with another Hoyt function, the resulting distribution has the same mathematical form, with a total width equal to the sum of the partial widths. Thus, a transition between two distinct atomic levels, e.g. the $K\alpha$ radiation, has a Hoyt intensity distribution, the width of which is the sum of the two levels involved. For the present experiments we have shown that effectively the electron transitions take place between an inner shell (Hoyt distribution) and the vacuum level of the spectrometer, $E_v$, which may be written as

$$E_v = E_F + \phi_{\text{spectr}} \tag{9}$$

and may be considered sharp for our purposes. The natural shape of a photo electron line is thus a Hoyt function, whose constituent widths are that of the exciting X-radiation and that of the initial level. Deviations from this shape are due to (i) scattering of electrons in the source and (ii) the spectrometer window curve.

(i) *Electron scattering*

The phenomena of electron scattering in thin metal films have been given a great deal of attention in the last years. Apart from electron-atom collisions, resulting in some elastic scattering with small losses of energy, considerable inelastic scattering has been observed, manifesting itself in a series of satellites on the low energy side

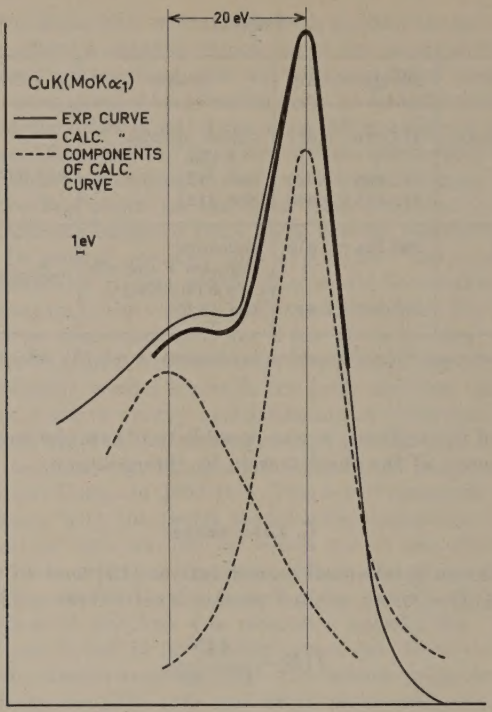



Fig. 6. Attempt to resolve the Cu$K$(Mo$K\alpha_1$) photo line into a line of unscattered electrons and a satellite due to inelastic scattering.

of a parent line. Some of the discrete energy losses have been attributed to the excitation of quantized oscillations of the electron plasma in the valence band. These energy losses are intermingled with events that must be ascribed to single particle excitation. Since an electron may undergo successive inelastic scattering, we might expect each mode of plasma- or particle excitation to give rise to several satellite lines, the intensities of which depend on the source thickness and the scattering mean free path of the electron. The scattering probability as well as the predominant mode of excitation may vary from substance to substance. A review of the present status of this field of research is given in ref. [14]. For many metals (e.g.Mn, Fe, Co, Ni, Au and Pt) the dominating energy loss quantum is about 20 eV and the corresponding excitation state has considerable width. Under these circumstances it has usually not been possible in the present work to completely resolve the undisturbed photo electron peaks from the satellites due to inelastic scattering, nor has it been possible to distinguish more than one satellite. To study the effects that the unresolved satellites may have on the photo line peaks, the Cu$K$(Mo$K\alpha_1$) line was examined. Fig. 6 shows this line, taken with a thin source, so that the satellite is not extremely pronounced. The discrete energy loss spectrum of Cu is well established [15], the predominant mode of excitation corresponding to 20 eV and the width of

the excitation state being 17 eV. To obtain the width of the satellite one must also take into consideration the width of the parent line, which in the present case is about 12 eV. Assuming that the widths add linearly we get for the satellite that $\Gamma \simeq 15$ eV and, for the parent line, that $\Gamma \simeq 6$ eV. Assuming further that both lines can be represented by Hoyt functions we then find that the shift of the parent line peak due to the unresolved satellite is

$$\Delta E = -0.4\, A \text{ eV}, \tag{10}$$

where $A$ is the ratio between the satellite- and the parent line amplitudes. The heavy curve in fig. 6 shows the sum of the two Hoyt functions with $A = 0.6$. It is seen that this curve is in good agreement with the experimental one. (The slow descent of the experimental curve on the low energy side of the satellite is probably due to successive events of inelastic scattering, which have no influence on the parent line.) The peak shift is then in this case 0.2 eV. It was found that all the photo lines resulting from conversion of Mo $K\alpha$ radiation were rather similar in appearance and expression (10) may therefore be assumed to give the right order of magnitude of the shift for all the cases studied. Although evaporated sources were used throughout this investigation the sources were usually thicker than the one employed for fig. 6, but in no case was $A$ found to exceed 1. Since the shift occurred in the calibration line as well as in the "unknown" line the errors introduced are only of the order of 0.1 eV and have been neglected.

(ii) *Spectrometer window*

The spectrometer window curve is most conveniently studied with a line, whose distortion due to electron scattering is negligible. To achieve this condition we must strive for improved resolution without changing the spectrometer setting. If we choose

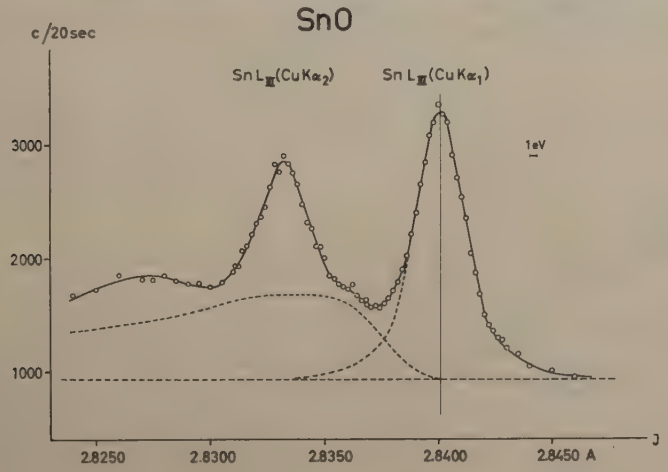



Fig. 7. Sn$L_{III}$(Cu$K\alpha_{1,2}$) doublet from thin layer of SnO. The natural line width is so small that the "undisturbed" peak is almost resolved from the satellite. The undisturbed lines are symmetric, indicating a symmetric spectrometer window.

a photo line resulting from conversion of an X-ray line that is considerably narrower than the Mo $K\alpha_1$ radiation, we may hope to be able to resolve the undisturbed photo peak from the satellite lines, particularly if we choose a converter with a low inelastic scattering cross-section. This latter condition is fulfilled by SnO.[1] The photo doublet $\mathrm{Sn}L_{\mathrm{III}}(\mathrm{Cu}\,K\alpha_{1,2})$ from SnO is shown in fig. 7. It is seen that the undisturbed photo lines are very nearly symmetrical, indicating a symmetric spectrometer window. (Elastic scattering seems to be negligible. The slight asymmetry, 12 %, of the Cu $K\alpha$ radiation mentioned in ref. [1] is insignificant, the major part of the photo line width being due to instrument broadening.) Hence we may conclude that the peak of an undisturbed photo line corresponds to the maximum of the original Hoyt function, if we neglect the minor error due to unresolved satellite lines.

For a given geometry, the instrument resolution for an iron-free spectrometer, $\Delta B\varrho/B\varrho$, is constant, $\Delta B\varrho$ being the half-width of the spectrometer window curve. From this point of view it is most desirable to work in as low an energy region as possible. An advantage of the present method is that one can choose the photo line energy by making a suitable choice of X-radiation: the lower the energy of the incoming radiation the more favourable will be the spectrometer width. To this comes the fact that the X-radiation line width is usually smaller the softer the radiation. The low energy limit for the photo lines is set by the cut-off of the Geiger detector, which in the present case lay around 2 keV. Throughout this investigation the Mo $K\alpha_1$ radiation was used to provide the excitation energy. This placed the photo lines in a suitable energy region. Another great advantage is the fact that the Mo $K\alpha_1$ line has been measured very accurately and has lately been proposed as a wave-length standard in X-ray spectroscopy [17].

### D. *Use of infinitely thick sources*

From the above one is led to expect that in certain favourable cases, when the natural line width and the instrument window permit sufficient resolution, the

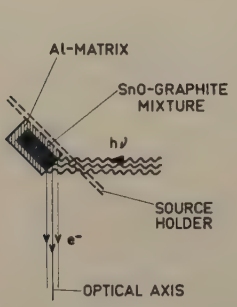



Fig. 8. Source geometry for infinitely thick samples.

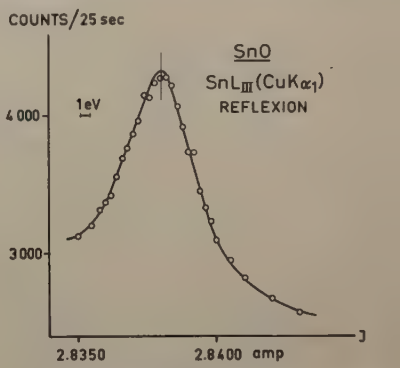



Fig. 9. $\mathrm{Sn}L_{\mathrm{III}}(\mathrm{Cu}\,K\alpha_1)$ line from infinitely thick source of SnO. The greater width as compared to the lines in fig. 7 is due to a greater source width.

[1] SnO is considered to be a semiconductor [16].

source thickness is immaterial in electron spectroscopy, the scattered electrons going into the resolved satellite lines. This would open entirely new possibilities for the present method of studying electron binding energies. Thus, for chemical shift studies the need for evaporated sources is a serious limitation, since it is difficult to control the chemical composition of thin films.

The SnO source used for fig. 7 was made by heating an evaporated Sn sample to 200°C for twelve hours. For comparison an infinitely thick SnO source was prepared out of SnO powder. In order to reduce the porosity of the sample, a slurry was made of SnO and graphite powder in alcohol, which was then packed into an aluminium matrix, 0.50 mm wide and 1 mm deep. This procedure gave rather dense and homogeneous samples. The source was exposed to the X-ray beam as illustrated in fig. 8. Fig. 9 shows the resulting $\mathrm{Sn}L_{\mathrm{III}}(\mathrm{Cu}\,K\alpha_1)$ photo line. It is seen that the line differs little from the undisturbed photo peak of the evaporated source, the only disadvantage being the higher background. (These results might be applied to low energy studies in conventional $\beta$-spectroscopy where one is usually concerned with the dual problem of thin sources and high activity.)

## IV. Experimental results

All the momentum values listed below have been corrected for the effective residual magnetic field. The conversion from momentum to energy was carried out with the aid of the tables in ref. [11]. In those cases where the accuracy of the tables did not suffice higher order interpolation was used. To obtain the quantity (B.E. $+\phi_{\mathrm{sp}}$) the mean energy $\bar{E}$ was subtracted from the energy of the Mo $K\alpha_1$ radiation. The latter was taken from ref. [1] to be 707.831 X.U., or, using the conversion constants given by DuMond and Cohen in 1953, 17479.0 eV.

The errors given for $\bar{E}$ are the mean errors obtained from the deviations from $\bar{E}$. In the quantity (B.E. $+\phi_{\mathrm{sp}}$) the (systematic) errors in the calibration lines have been included. The uncertainties in the elementary constants have not been taken into account.

All energy determinations were made on several samples which had been prepared independently. In those cases where oxidation or other contamination could be suspected the composition of the samples was examined by means of electron diffraction (see section V B).

### A. *Fourth period elements*

#### I. Mn

*Table 2.* Mn $K$(Mo $K\alpha_1$).

| Calibration line | Mean current $\bar{I}$ (amps) | $B\varrho$ (gauss-cm) | $E$ (eV) | Deviation fr. $\bar{E}$ (eV) |
|---|---|---|---|---|
| Cu $K$(Mo $K\alpha_1$); $\bar{I}_c = 4.09158$ amps | 4.64754 | 354.498 | 10935.0 | +0.1 |
| | | 354.503 | 10935.3 | +0.4 |
| | | 354.481 | 10934.0 | −0.9 |
| | | 354.499 | 10935.1 | +0.2 |

$\bar{E}$: $10934.9 \pm 0.3$ eV

Mn $K$: B.E. $+\phi_{\mathrm{sp}} = 6544.1 \pm 0.8$ eV

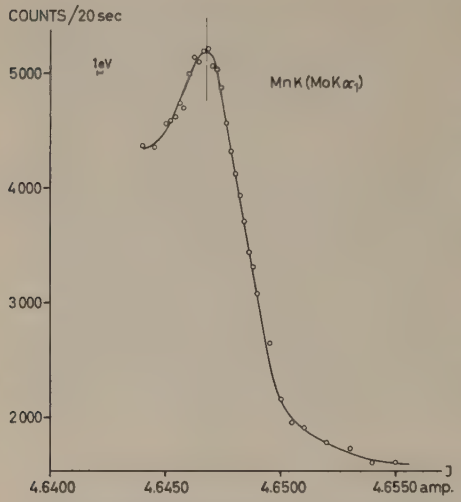



Fig. 10. Mn $K$(Mo $K\alpha_1$) photo line.

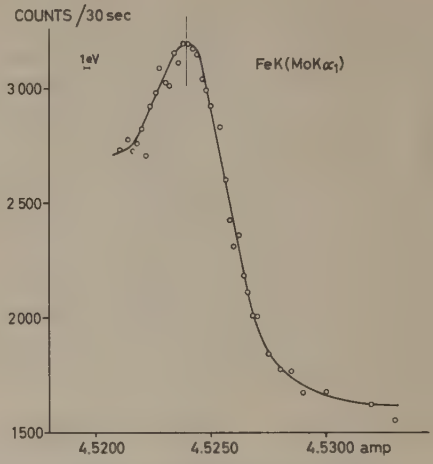



Fig. 11. Fe $K$(Mo $K\alpha_1$) photo line.

## II. Fe

*Table 3.* Fe $K$(Mo $K\alpha_1$).

| Calibration line | Mean current $\bar{I}$ (amps) | $B\varrho$ (gauss-cm) | $E$ (eV) | Deviation fr. $\bar{E}$ (eV) |
|---|---|---|---|---|
| Cu $K$(Mo $K\alpha_1$); $\bar{I}_c = 4.09330$ amps | 4.52386 | 344.924 | 10358.0 | +0.4 |
| | | 344.913 | 10357.3 | −0.3 |
| | | 344.921 | 10357.8 | +0.2 |
| | | 344.914 | 10357.4 | −0.2 |

$\bar{E}$: 10357.6 ± 0.2 eV

Fe $K$: B.E. + $\phi_{sp}$ = 7121.4 ± 0.7 eV

## III. Co

*Table 4.* Co $K$(Mo $K\alpha_1$).

| Calibration line | Mean current $\bar{I}$ (amps) | $B\varrho$ (gauss-cm) | $E$ (eV) | Deviation fr. $\bar{E}$ (eV) |
|---|---|---|---|---|
| Cu $K$(Mo $K\alpha_1$); $\bar{I}_c = 4.09258$ amps | 4.39049 | 334.808 | 9764.9 | +0.2 |
| | | 334.809 | 9765.0 | ±0.0 |
| A6; $\bar{I}_c = 3.71980$ amps | 4.38847 | 334.814 | 9765.2 | +0.2 |
| | | 334.805 | 9764.7 | −0.3 |

$\bar{E}$: 9765.0 ± 0.1 eV

Co $K$: B.E. + $\phi_{sp}$ = 7714.0 ± 0.7 eV

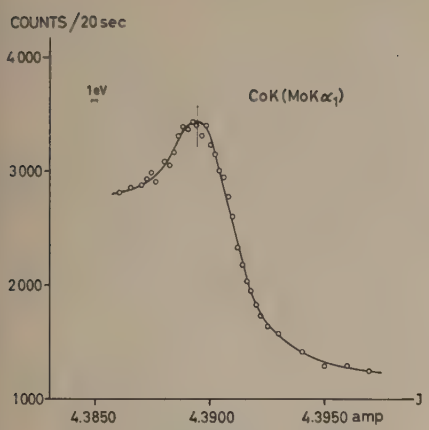



Fig. 12. Co $K$(Mo $K\alpha_1$) photo line.

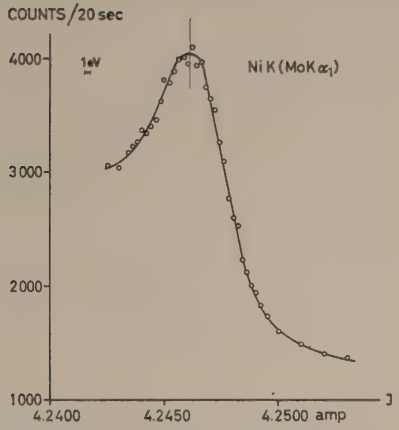



Fig. 13. Ni $K$(Mo $K\alpha_1$) photo line.

## IV. Ni

*Table 5.* Ni $K$(Mo $K\alpha_1$).

| Calibration line | Mean current $\bar{I}$ (amps) | $B\varrho$ (gauss-cm) | $E$ (eV) | Deviation fr. $\bar{E}$ (eV) |
|---|---|---|---|---|
| Cu $K$(Mo $K\alpha_1$); $\bar{I}_c = 4.09097$ amps | 4.24496 | 323.843 | 9141.3 | +0.1 |
| | | 323.845 | 9141.4 | +0.2 |
| | | 323.826 | 9140.4 | −0.8 |
| A6; $\bar{I}_c = 3.72092$ | 4.24610 | 323.851 | 9141.7 | +0.5 |

$\bar{E}$: 9141.2 ± 0.3 eV

Ni $K$: B.E. + $\phi_{sp}$ = 8337.8 ± 0.7 eV

## B. *Sixth period elements*

## I. Ir

*Table 6.* Ir $L_{III}$(Mo $K\alpha_1$).

| Calibration line | Mean current $\bar{I}$ (amps) | $B\varrho$ (gauss-cm) | $E$ (eV) | Deviation fr. $\bar{E}$ (eV) |
|---|---|---|---|---|
| Cu $K$(Mo $K\alpha_1$); $\bar{I}_c = 4.08946$ amps | 3.50638 | 267.581 | 6258.4 | −0.8 |
| | | 267.625 | 6260.5 | +1.3 |
| | | 267.598 | 6259.2 | ±0.0 |
| | | 267.582 | 6258.5 | −0.7 |

$\bar{E}$: 6259.2 ± 0.5 eV

Ir $L_{III}$: B.E. + $\phi_{sp}$ = 11219.8 ± 0.6 eV

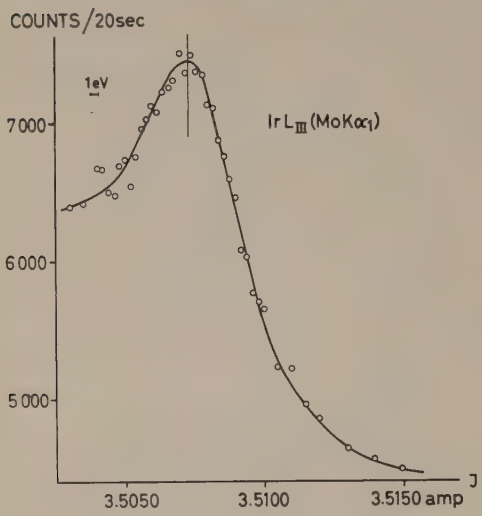



Fig. 14. Ir$L_{III}$(Mo$K\alpha_1$) photo line.

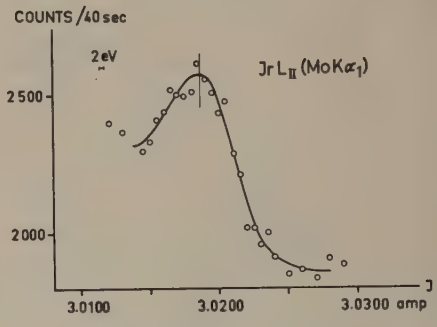



Fig. 15. Ir$L_{II}$(Mo$K\alpha_1$) photo line.

*Table 7.* Ir $L_{II}$(Mo $K\alpha_1$).

| Calibration line | Mean current $\bar{I}$ (amps) | $B\varrho$ (gauss-cm) | $E$ (eV) | Deviation fr. $\bar{E}$ (eV) |
|---|---|---|---|---|
| Cu $K$(Mo $K\alpha_1$); $\bar{I}_c = 4.08935$ amps | 3.01950 | 230.470<br>230.426 | 4650.1<br>4648.3 | +0.4<br>−1.4 |
| (1) | — | — | 4650.6 | +0.9 |

$\bar{E}$: 4649.7 ± 0.7 eV

[1] This value was obtained by subtracting from $\bar{E}$ for Ir $L_{III}$(Mo $K\alpha_1$) the energy difference between Ir $K\alpha_1$ and Ir $K\alpha_2$ as given by Ingelstam [18]

Ir $L_{II}$: B.E. + $\phi_{sp}$ = 12829.3 ± 0.8 eV

## II. Pt

*Table 8.* Pt $L_{III}$(Mo $K\alpha_1$).

| Calibration line | Mean current $\bar{I}$ (amps) | $B\varrho$ (gauss-cm) | $E$ (eV) | Deviation fr. $\bar{E}$ (eV) |
|---|---|---|---|---|
| Cu $K$(Mo $K\alpha_1$); $\bar{I}_c = 4.09156$ amps | 3.40856 | 259.999<br>259.997<br>259.999<br>259.995 | 5910.8<br>5910.7<br>5910.8<br>5910.6 | +0.1<br>±0.0<br>+0.1<br>−0.1 |

$\bar{E}$: 5910.7 ± 0.1 eV

Pt $L_{III}$: B.E. + $\phi_{sp}$ = 11568.3 ± 0.2 eV

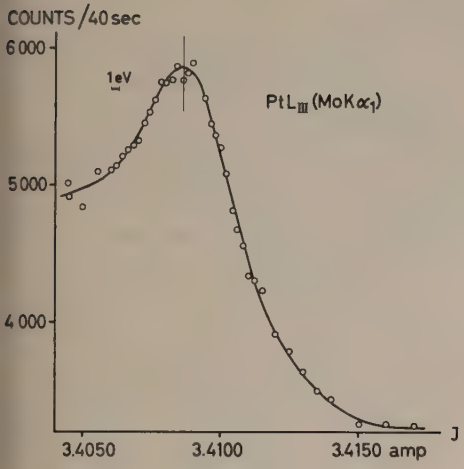



Fig. 16. Pt$L_{III}$(Mo$K\alpha_1$) photo line.

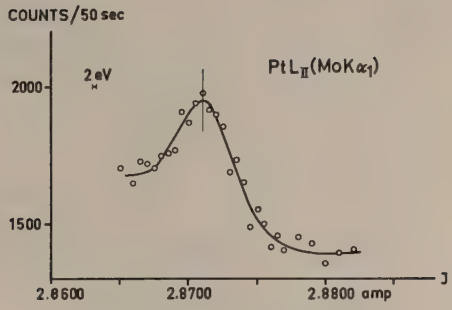



Fig. 17. Pt$L_{II}$(Mo$K\alpha_1$) photo line.

*Table 9.* Pt $L_{II}$(Mo $K\alpha_1$).

| Calibration line | Mean current $\bar{I}$ (amps) | $B\varrho$ (gauss-cm) | $E$ (eV) | Deviation fr. $\bar{E}$ (eV) |
|---|---|---|---|---|
| Cu $K$(Mo $K\alpha_1$); $\bar{I}_c = 4.09140$ amps | 2.87127 | 219.026 | 4201.5 | −0.2 |
| (1) | — | — | 4201.9 | +0.2 |

$\bar{E}$: 4201.7 ± 0.2 eV

[1] This value was obtained by subtracting from $\bar{E}$ for Pt $L_{III}$(Mo $K\alpha_1$) the energy difference between Pt $K\alpha_1$ and Pt $K\alpha_2$ as given by Ingelstam [18]

Pt $L_{II}$: B.E. + $\phi_{sp}$ = 13278.3 ± 0.4 eV

## III. Au

*Table 10.* Au $L_{III}$(Mo $K\alpha_1$).

| Calibration line | Mean current $\bar{I}$ (amps) | $B\varrho$ (gauss-cm) | $E$ (eV) | Deviation fr. $\bar{E}$ (eV) |
|---|---|---|---|---|
| Cu $K$(Mo $K\alpha_1$); $\bar{I}_c = 4.08995$ amps | 3.30257 | 252.006 | 5554.9 | −0.3 |
| | | 252.012 | 5555.2 | ±0.0 |
| | | 252.029 | 5555.9 | +0.7 |
| | | 252.011 | 5555.1 | −0.1 |
| | | 252.006 | 5554.9 | −0.3 |

$\bar{E}$: 5555.2 ± 0.2 eV

Au $L_{III}$: B.E. + $\phi_{sp}$ = 11923.8 ± 0.4 eV

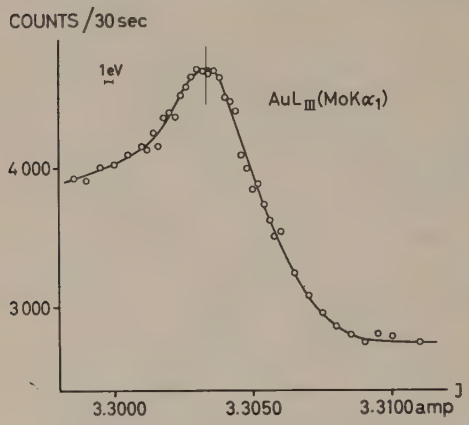



Fig. 18. Au$L_{III}$(Mo$K\alpha_1$) photo line.

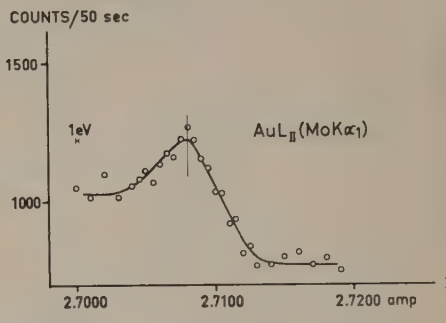



Fig. 19. Au$L_{II}$(Mo$K\alpha_1$) photo line.

*Table 11.* Au $L_{II}$(Mo $K\alpha_1$).

| Calibration line | Mean current $\bar{I}$ (amps) | $B\varrho$ (gauss-cm) | $E$ (eV) | Deviation fr. $\bar{E}$ (eV) |
|---|---|---|---|---|
| Cu $K$(Mo $K\alpha_1$); $\bar{I}_c = 4.08983$ amps | 2.70750 | 206.616<br>206.614 | 3740.6<br>3740.6 | +0.1<br>+0.1 |
| (1) | — | — | 3740.4 | −0.1 |

$\bar{E}$: 3740.5 ± 0.1 eV

1 This value was obtained by subtracting from $\bar{E}$ for Au $L_{III}$(Mo $K\alpha_1$) the energy difference between Au $K\alpha_1$ and Au $K\alpha_2$ as given by Beckman *et al.* [19]. (If instead we use the value for the Au $K\alpha$ doublet splitting given by Ingelstam [18] we obtain the value 3741.3 eV. However, Beckman claims higher accuracy than Ingelstam.)

Au $L_{II}$: B.E. + $\phi_{sp}$ = 13738.5 ± 0.3 eV

## IV. Hg

Making thin mercury samples proved somewhat problematic. The samples were finally prepared by bombarding the sample backings with Hg ions in a mass separator. This method was most successful when a thin ( ~ 100 Å) Au layer was pre-evaporated onto the backing. Thus, the values probably pertain to gold (g) or aluminium (a) amalgam.

*Table 12.* Hg $L_{III}$(Mo $K\alpha_1$).

| Calibration line | Mean current $\bar{I}$ (amps) | $B\varrho$ (gauss-cm) | $E$ (eV) | Deviation fr. $\bar{E}$ (eV) |
|---|---|---|---|---|
| Cu $K$(Mo $K\alpha_1$); $\bar{I}_c = 4.09208$ amps | 3.19325 | 243.541 (g) | 5189.8 | −0.1 |
| | | 243.558 (a) | 5190.5 | +0.6 |
| | | 243.548 (g) | 5190.1 | +0.2 |
| | | 243.530 (g) | 5189.3 | −0.6 |

$\bar{E}$: 5189.9 ± 0.3 eV

Hg $L_{III}$: B.E. + $\phi_{sp}$ = 12289.1 ± 0.4 eV

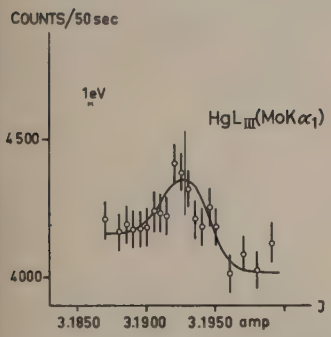



Fig. 20. Hg $L_{III}$(Mo $K\alpha_1$) photo line.

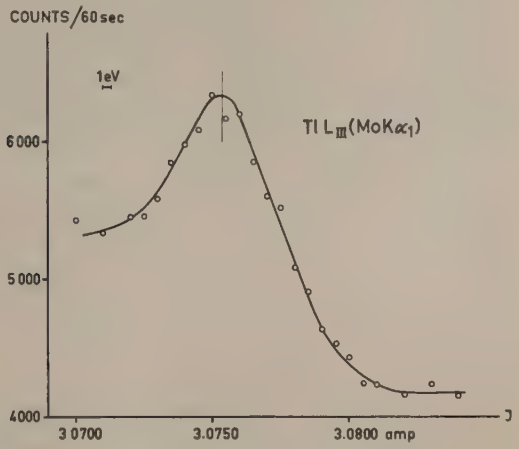



Fig. 21. Tl $L_{III}$(Mo $K\alpha_1$) photo line.

## V. Tl

*Table 13.* Tl $L_{III}$(Mo $K\alpha_1$).

| Calibration line | Mean current $\bar{I}$ (amps) | $B\varrho$ (gauss-cm) | $E$ (eV) | Deviation fr. $\bar{E}$ (eV) |
|---|---|---|---|---|
| Cu $K$(Mo $K\alpha_1$); $\bar{I}_c = 4.09156$ amps | 3.07589 | 234.617 | 4818.2 | −0.3 |
| | | 234.624 | 4818.4 | −0.1 |
| | | 234.630 | 4818.7 | +0.2 |
| | | 234.628 | 4818.6 | +0.1 |

$\bar{E}$: 4818.5 ± 0.1 eV

Tl $L_{III}$: B.E. + $\phi_{sp}$ = 12660.5 ± 0.3 eV

## VI. Pb

*Table 14.* Pb $L_{III}$(Mo $K\alpha_1$).

| Calibration line | Mean current $\bar{I}$ (amps) | $B\varrho$ (gauss-cm) | $E$ (eV) | Deviation fr. $\bar{E}$ (eV) |
|---|---|---|---|---|
| Cu $K$(Mo $K\alpha_1$); $\bar{I}_c = 4.09036$ | 2.95078 | 225.172 | 4439.6 | +0.8 |
| | | 225.133 | 4438.1 | −0.7 |
| | | 225.122 | 4437.6 | −1.2 |
| | | 225.181 | 4440.0 | +1.2 |
| A6; $\bar{I}_c = 3.71685$ amps | 2.94870 | 225.150 | 4438.7 | −0.1 |

$\bar{E}$: 4438.8 ± 0.5 eV

Pb $L_{III}$: B.E. + $\phi_{sp}$ = 13040.2 ± 0.6 eV

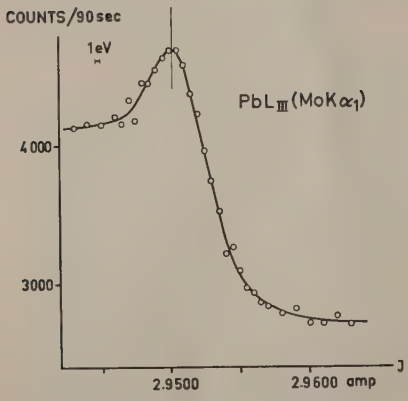



Fig. 22. Pb $L_{III}$(Mo $K\alpha_1$) photo line.

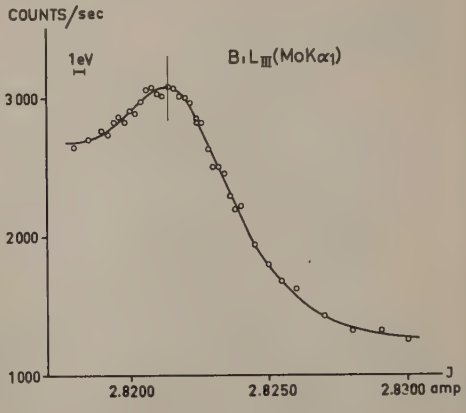



Fig. 23. Bi $L_{III}$(Mo $K\alpha_1$) photo line.

## VII. Bi

*Table 15.* Bi $L_{III}$(Mo $K\alpha_1$).

| Calibration line | Mean current $\bar{I}$ (amps) | $B\varrho$ (gauss-cm) | $E$ (eV) | Deviation fr. $\bar{E}$ (eV) |
|---|---|---|---|---|
| Cu $K$(Mo $K\alpha_1$); $\bar{I}_c = 4.09138$ amps | 2.82059 | 215.160 | 4055.1 | −0.4 |
| | | 215.173 | 4055.6 | +0.1 |
| | | 215.155 | 4055.9 | +0.4 |
| | | 215.163 | 4055.2 | −0.3 |

$\bar{E}$: 4055.5 ± 0.2 eV

Bi $L_{III}$: B.E. + $\phi_{sp}$ = 13423.5 ± 0.3 eV

### C. *Work function correction*

The fact that the work function of the spectrometer enters the measured binding energy must at first be considered a drawback of the present method, the work function being sensitive to the composition of the material, the degree of out-gassing, etc. However, the reproducibilities of the measured energies over more than one year rendered sufficient proof that $\phi_{sp}$ had reached its equilibrium value and remained constant. Hence the most serious objection is eliminated. Since the copper tank of the spectrometer was undoubtedly oxidized to some extent, the work function of Cu, given in the literature, could not be used off-hand. Also, work functions have usually been measured with extremely good vacuum and highest degree of purity. A value pertaining more directly to the present conditions was therefore desirable. An auxiliary piece of apparatus was constructed for the study of contact potentials by means of the Kelvin method.[1] The apparatus was essentially that described by Zisman [20]. However, in the present case the design was simplified for use at atmospheric pressure only. The metals to be studied were applied to the two plates of a parallel plate condenser, one of which was kept fixed while the other was attached to a pair of springs, which allowed it to vibrate. Vibrations were induced by a piano wire, in which standing waves were excited by means of a narrow stream of compressed air. If there exists a potential difference between the condenser plates, an A.C. signal appears across the plates, the amplitude of which can be approximated by the expression

$$V_{max} = \frac{V_0 \varkappa_0 A \omega d_1}{d_0^2 (R^2 C^2 \omega^2 + 1)} . \qquad (11)$$

Here, $V_0$ = the potential difference between the plates;
$\varkappa_0$ = the permittivity;
$A$ = the area of the plates;
$d_1$ = the vibration amplitude;
$\omega$ = the vibration frequency;
$d_0$ = the equilibrium distance between the plates;
$C \simeq \varkappa_0 (A/d_0)$ = the plate capacitance;
$R$ = the resistance across the plates.

Ordinarily, $V_0$ equals the contact potential $\Delta\phi$ between the two plates. To measure $\Delta\phi$, one connects a variable countervoltage across the condenser. When the contact potential is exactly balanced, the A.C. signal disappears.

Contact potentials were measured for many metals known to be fairly resistant to oxidation, and were in no case found to differ widely from the values given in the literature [21]. From this we may conclude that measuring contact potentials in air does not introduce a serious error.

Hagström [22] has measured the photo-electric work function of freshly evaporated Ag in a vacuum of the same degree as used in the spectrometer. He found that $\phi_{Ag}$ equals 4.65 eV. Next, the contact potential between freshly evaporated layers of Cu and Ag was measured and found to be 0.15 eV towards lower work function in Cu. It was further found that the contact potential was zero between freshly evaporated Cu and Cu that had been subjected to natural ageing. (If one Cu plate was heated to 200°C for twelve hours so that a visible layer of CuO was formed, a

[1] This work was done together with fil. lic. C. Nordling.

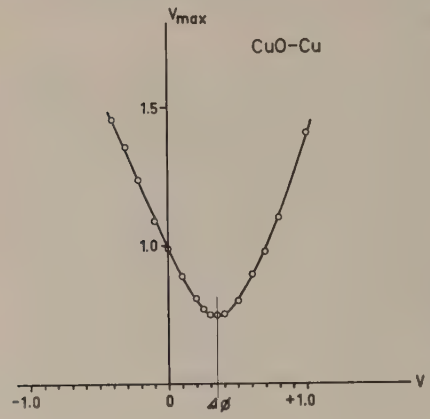



Fig. 24. Determination of contact potential, $\Delta\phi$, between CuO and Cu. The curve shows the amplitude of the A.C. signal across the condenser plates, $V_{max}$, as a function of the D.C. counter voltage $V$. The shape of the curve depends on the characteristics of the amplifier stages after the condenser.

contact potential of 0.35 eV appeared, as seen in fig. 24). For the work function of naturally aged Cu (spectrometer material) we thus get the value

$$\phi_{sp} = 4.5 \pm 0.3 \text{ eV}.$$

Table 16 gives the binding energies, B.E., with the work function correction applied.

*Table 16.*

| Shell | B.E. (eV) | Shell | B.E. (eV) |
|---|---|---|---|
| Mn $K$ | 6539.6 | Pt $L_{III}$ | 11563.8 |
| Fe $K$ | 7116.9 | Pt $L_{II}$ | 13273.8 |
| Co $K$ | 7709.5 | Au $L_{III}$ | 11919.3 |
| Ni $K$ | 8333.3 | Au $L_{II}$ | 13734.0 |
| Cu $K$ | 8979.2 | Hg $L_{III}$ | 12284.6 |
| | | Tl $L_{III}$ | 12656.0 |
| Ir $L_{III}$ | 11215.3 | Pb $L_{III}$ | 13035.7 |
| Ir $L_{II}$ | 12824.8 | Bi $L_{III}$ | 13419.0 |

## V. Discussion of results

### A. *The modified Moseley diagram*

If the square root of the energy of a given X-ray transition, $\sqrt{\nu/R}$, is plotted against the atomic number $Z$, the resulting curve is an approximately straight line. This empirical fact was first noted by Moseley and constitutes one of the first systematic relations observed in X-ray spectroscopy. If the main linearity is eliminated by subtracting from $\sqrt{\nu/R}$ a suitable function $aZ + b$, we obtain a so-called "modified Moseley diagram", which makes possible a more detailed study of the higher terms

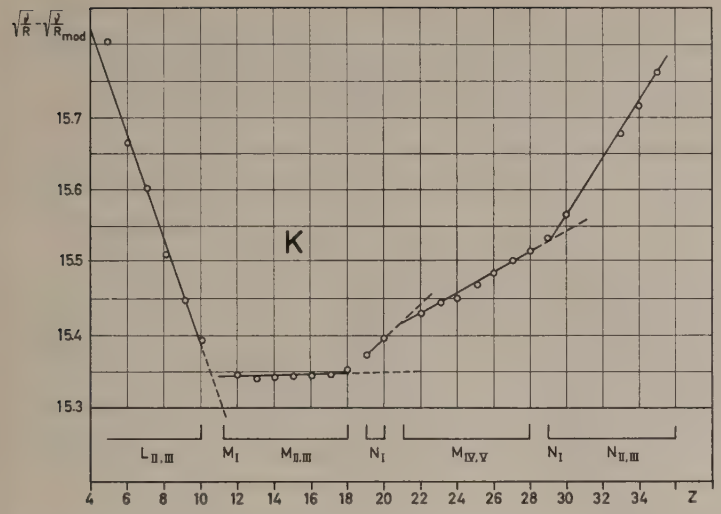



Fig. 25. Modified Moseley diagram of $K$ binding energies, plotted with X-ray data. Note that the energy scale is considerably reduced compared with figs. 27 and 28. (After Idei [24].)

in the transition energy. As the nature of atomic transitions became better understood it was possible, with the aid of quantum mechanics, to give a qualitative theoretical explanation of the Moseley diagrams and their higher order deviations from straight lines in terms of relativity-, spin-, and screening effects [23]. However, the models used so far have been too crude to give quantitative agreement with the experimental results. Generally speaking, the function $\sqrt{\nu/R}$ can be expressed as a power series in $Z$, the coefficients of which are functions of the quantum numbers characteristic of the states involved in the transition. From this it follows that the modified Moseley diagram of a given transition (e.g. the $K\alpha_1$ transition) should yield a smooth function. This has been verified empirically [1].

If instead we follow the *binding energy* of a given atomic shell through the periodic table, the situation is a different one, the binding energy corresponding to a transition from the given shell to the lowest unoccupied level in the atom. Here, the quantum numbers of the final state vary, and we must expect a discontinuity in the modified Moseley diagram each time an outer shell is filled and the symmetry of the lowest unoccupied level is changed. This, too, is in rough agreement with the results of X-ray spectroscopy, as shown by Idei (ref [24], see fig. 25). The higher order terms are so small that they are not detectable in the small ranges of $Z$, over which the function is continuous.

In our discussion so far we have assumed that we are dealing with free atoms, where the initial and final states can be uniquely described by the usual set of quantum numbers. In the case of a crystalline solid the situation becomes more complicated: by the atomic interaction the outer energy levels are broadened into bands, which have lost their pure symmetry character. Usually a band is designated by the main symmetry (i.e. that of the corresponding level in the free atom), but

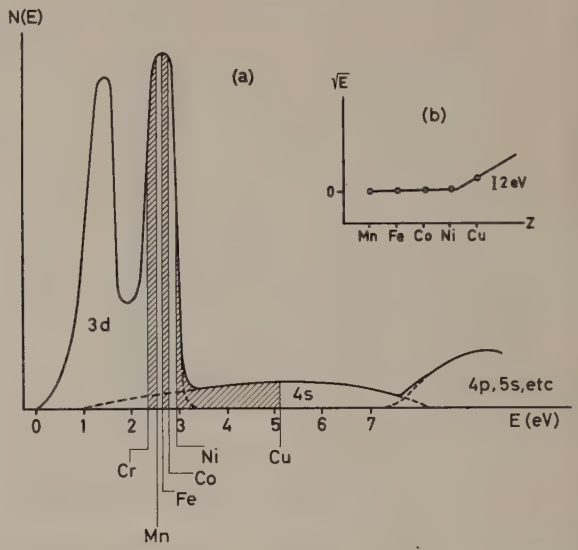



Fig. 26. (*a*) Calculated band structure of metallic Cu. The level density curve, $N(E)$, taken from ref. [27], is a composite sketch from many different calculations, which may be exemplified by ref. [26] and [31]. (*b*) Variations of the Fermi level energy with $Z$, due to the variation in level density. It has been assumed that the calculated band structure of Cu is valid throughout this region of $Z$.

we must keep in mind that the wave function characteristic of the band is "hybridized":

$$\psi(nl) = A\psi_s + B\psi_p + C\psi_d + \cdots, \tag{12}$$

where the subscripts indicate the symmetry of the partial wave functions [25]. The broadening of the bands depends on the structure and cell constants of the crystal. It is usual that bands of different origin in the free atom overlap considerably in the solid [31]. The density of states in a band can be expected to vary with energy. For modified Moseley diagrams of electron transitions to the Fermi surface in a solid we must therefore expect an energy variation that depends on the main symmetries represented in the band, in which the Fermi level is located, as well as on the density of states.

In the quantitative theoretical work that exists on this subject, the fourth period elements have been treated most extensively. Fig. 26 shows the band structure calculated for metallic Cu (cubic crystal field) [27]. We shall for a moment assume that the same band structure applies to the preceding elements Ni, Co, Fe and Mn, and consider only the effect of the varying density of states as we fill up the band. The 3*d* band, we know, holds ten electrons per atom, the 4*s* band two, etc. If we divide the 3*d* band into ten equal surfaces (fig. 26*a*) we find that the Fermi level energy increases rather monotonously, despite the variation in level density, until we reach the element Cu, where the energy of the Fermi surface makes an abrupt jump due to the low level density in the 4*s* band (fig. 26*b*).

The limitations of the above reasoning are obvious. Firstly, we have neglected the energy variation due to variations in the final state symmetry. If the band structure given in fig. 26*a* is approximately correct, this effect might be expected to accentuate the discontinuity at Cu. (This discontinuity should also occur in the

case of of a free atom, since the Fermi surface changes from $3d$ to $4s$ symmetry). If, however, the overlapping of the $3d$ and $4s$ bands is greater than suggested by fig. $26a$, the discontinuity might shift towards higher $Z$. Secondly, we have assumed the band structure calculated for Cu to be valid for all the elements Ni, Co, Fe and Mn, despite the fact that the calculations pertain to cubic crystal fields and should give different results for different cell constants. If these latter circumstances were given due consideration we might find more irregularities in the energy as a function of $Z$.

### B. *Experimental considerations*

In figures 27 and 28 the present results are given in the form of modified Moseley diagrams, together with representative X-ray data. Before attaching any fundamental importance to the discrepancies between the present and the X-ray results, we must eliminate the possibility of an explanation in terms of experimental errors.

Fig. 27 shows the modified Moseley diagram for the $K$ binding energies of the fourth period elements. Except for Co and Cu, the energies obtained in the present work are higher than the X-ray values. It is to be noted that the three sets of X-ray values for the elements Mn, Fe, Co and Ni form nearly perfect straight and parallel lines, indicating great relative accuracy. (Of the three groups of X-ray data, those of Beeman *et al.* [28] and of Sanner [29] are probably the most reliable.) For the present energy values, a straight line, parallel to those of the X-ray data but displaced by about 2.5 eV, can be drawn through the values for Mn and Ni. It should be noted that this line also passes through the point for Cu. (See section VC). However, the Fe and Co values deviate markedly, and in the opposite sense, from this line.

The elements Fe, Co and Ni are ferromagnetic, and we must examine the possibility that a layer of ferromagnetic material, however thin, might cause a shift in an electron line. In view of the fact that a perturbing magnetic field in the vicinity of the source has little influence on the line position (see section IIIA) this possibility seemed small. To eliminate it, a basic iron layer was evaporated onto the middle section of the source holder, after which copper was evaporated onto all three sections. The Cu $K$(Mo $K\alpha_1$) lines from all three sections were then measured. The iron base was found to have no effect on the line from the middle section.

In ref. [4] Nordling, Sokolowski and Siegbahn have examined the $K$ binding energy of Cu in $Cu_2O$ and CuO as compared to the binding energy in the pure metal. A "chemical" shift of as much as 4.4 eV was observed for the higher oxide, stressing the importance of pure metallic sources for the present investigation. Electron diffraction offers the best tool for the analysis of extremely thin crystalline films. Electron microscope sources, prepared simultaneously with and of the same thickness as the spectrometer samples, were therefore examined for possible oxide contamination. The electron diffraction studies also provided a check of the crystal structure of the thin metallic films. Ag and MgO were used as calibration substances. The lattice constants obtained for the different reflexes were compared to those listed for the metal planes in the ASTM card catalogue [33]. It was found that if the samples were exposed to air for a minimum of time during the transfer from the evaporation chamber to the vacuum of the spectrometer (electron microscope) no oxidation could be detected. The crystal structure was in all cases found to be the one listed as normal for the metals in question. In one case (Bi) some degree of crystal orientation was observed in the evaporated film. Fig. 29 gives some of the diffraction patterns and the Miller indices for those metal reflexions that could be identified. In most

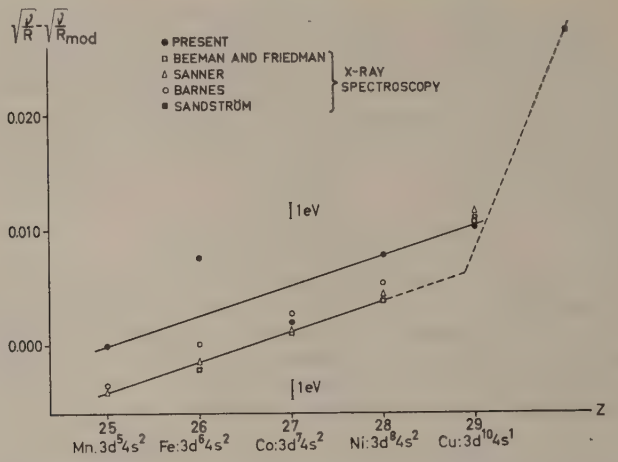



Fig. 27. Modified Moseley diagram for the $K$ binding energies of the fourth period elements. The X-ray data are taken from ref. [28], [29], [30] and [1]. The electron configurations given pertain to the free atoms.

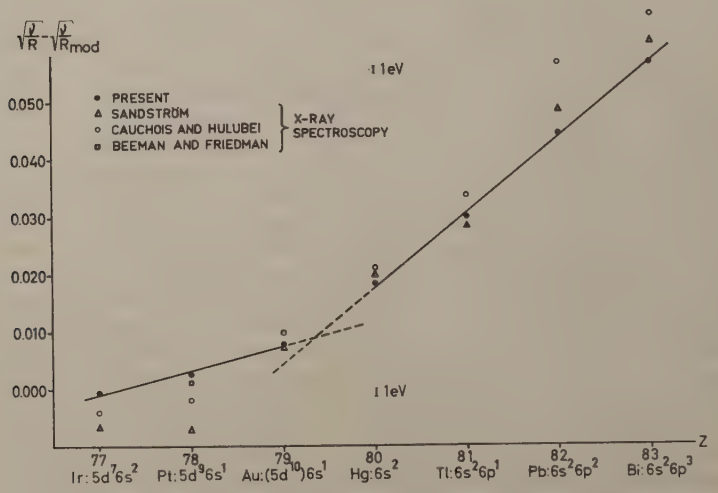



Fig. 28. Modified Moseley diagrams for the $L_{III}$ binding energies of the sixth period elements. The X-ray data are those given in ref. [1], [36] and [28].

cases additional reflexions (with large ring diameters) were observed that originated in planes of smaller lattice constants than the smallest ones listed in the ASTM card catalogue. However, no rings were found between the identified metal reflexions, that must be attributed to oxide impurities. We must conclude that the irregularities in

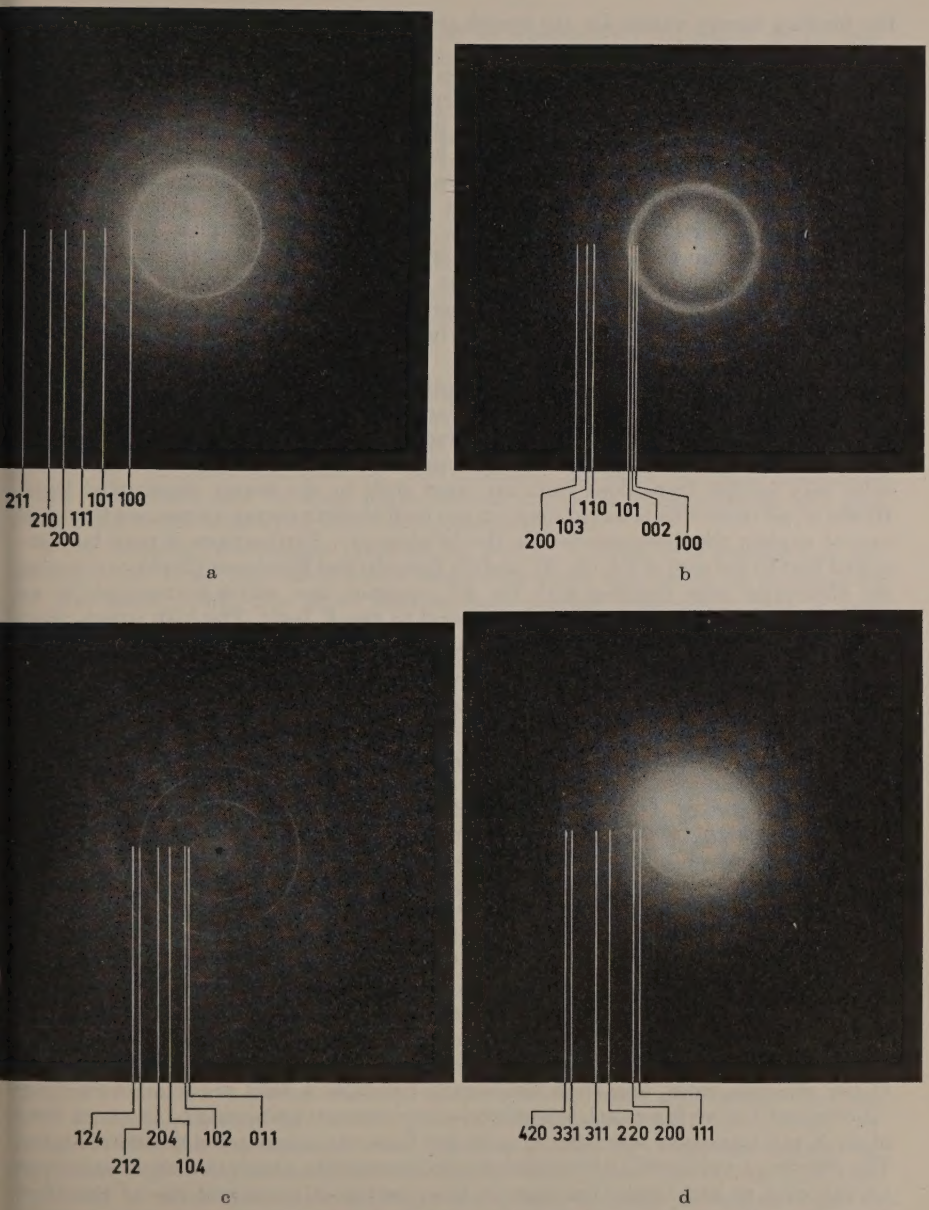



Fig. 29. Electron diffraction patterns of thin metal films. (*a*) Fe: bcc, $a_0 = 2.8664$ Å. (*b*) Co: hex., $a_0 = 2.501$ Å, $c_0 = 4.066$ Å. (*c*) Bi: hex., $a_0 = 4.546$ Å, $c_0 = 11.860$ Å. The sample shows some degree of orientation. (*d*) Pb: fcc, $a_0 = 4.9506$ Å.

the binding energy values for the fourth period elements cannot be given a trivial explanation.

Fig. 28 shows a modified Moseley diagram for the $L_{III}$ binding energies of the sixth period elements. Since here the X-ray absorption edges correspond to higher energies than the $K$ absorption edges of the fourth period elements, it is to be expected that the accuracy of the X-ray data is poorer here. This is illustrated by the fact that the scattering of the X-ray values is more pronounced. For the present measurements, the situation is the converse, since the $L_{III}$ photo lines of the sixth period elements fall at very low energies. For the elements with incomplete $d$ shells in the fourth as well as in the sixth period, the present data show a systematic tendency towards higher values as compared to the X-ray data. However, the converse is true for the elements Hg, Pb, Tl and Bi. Therefore, the discrepancies cannot very well be attributed to systematic errors, e.g. in the work function or residual field corrections.

The most common errors in X-ray absorption studies have been discussed in many papers [1, 27]. We might mention the displacement of the absorption edge caused by thick sources [34]. Also, poor instrument resolution can make it difficult to separate the initial rise of the edge from the subsequent Kossel structure. Finally, selection rules may inhibit transitions from an inner shell to the lowest unoccupied level. However, all these effects would result in too high binding energy values and therefore cannot explain the discrepancies for the $3d$ elements. Furthermore it may be mentioned that in the case of Fe, Co, Ni, and Cu Beeman and Friedman (28) have recorded the absorption edge together with the $K\beta_5$ emission line, which corresponds to an electron transition from the conduction band to the $K$ level. The high energy limit of the emission line, thought to correspond to a transition from the Fermi level, was found to coincide with the absorption edge, which leaves little doubt about the correct interpretation of the X-ray data.

### C. *Conclusions*

In view of section V A we find that the modified Moseley diagram for the $K$ binding energies of Mn to Cu, if plotted with X-ray data, is consistent with the free atom model but can, under specific assumptions, also be brought into accordance with band theory. If we consider a similar plot with the present data, we find deviations from the regularity of the X-ray values, which are not ruled out by more general theoretical considerations.

The discrepancies that exist in the data for the fourth period elements suggest that there is some fundamental difference in the "binding energies" determined by the two methods. The most obvious difference in the methods is that the transitions, giving rise to X-ray absorption edges, are governed by selection rules, whereas the processes detected in the present measurements are not (see section II). Because of the selection rules, and since the energy bands in a solid are characterized by "hybridized" wave functions, the effective level density pertaining to the final state in an X-ray transition will differ in principle from the calculated densities of states. The effective level density determines the structure of the absorption edge but cannot be expected to have great bearings on the position of the initial rise of the edge. If anything, the edge might be shifted towards higher energy, which would counteract the discrepancies.

Recently, Parratt [27] has proposed a mechanism for X-ray transitions, in terms

of which the differences in the results may be qualitatively explained. As an inne electron leaves its shell, the changing Coulomb field around the atom also affects the outer orbitals, which become more tightly bound to the nucleus. The valence electrons may adjust to the new Hamiltonian before the inner vacancy is filled or may remain in excited states. The influence of the incompletely screened nucleus on the outer electrons may depend on many factors, e.g. the main symmetry of the valence electrons and the electron mobility in the crystal. However, as long as there is such an influence the atom in which the electron transition takes place can be regarded as an impurity atom in the crystal lattice and may be expected to give rise to unoccupied energy levels below the Fermi surface of the crystal. If the original electron transition can go to one of these "impurity" levels the low energy values of the X-ray absorption edges can be accounted for. In the photo electron method the emitted electron can always be thought to go to the Fermi level of the complete crystal.

The mechanism described above stresses the danger of making uncritical use of the one-electron model, where we concern ourselves only with the initial and final states of the electron actually making the transition. All predictions made by means of this vast simplification must be very uncertain. However, no other practicable model is available and we must hope that the neglected interactions do not alter the general trends arrived at with the one-electron model.

If the transition mechanism proposed by Parratt is valid, it is perhaps not surprising if the X-ray data show trends resembling those that are to be expected for the free atoms, while the photo electron data provide information that is more relevant to the band structure of the undisturbed crystal. The irregularities exhibited by the modified Moseley diagram of the present data in fig. 27 show that the $K$ binding energy in the fourth period is a sensitive function of the crystal parameters. We have previously pointed out that a straight line can be drawn through the values for Mn, Ni and Cu. This line nearly coincides with the least squares fit to the whole set of data and may be taken to give the general trend of the $K$ binding energy from $Z = 25$ to $Z = 29$. Nordling [12] has measured the $K$ binding energies of the subsequent elements, Zn, Ga, etc., by means of the photo electron method. His measurements indicate a change in slope of the modified Moseley diagram between Cu and Zn rather than between Ni and Cu, as is the case for the X-ray data. As mentioned in section V A, this may suggest that the overlapping of the $3d$ and $4s$ bands is greater than calculated.

For the $L_{III}$ binding energies of the sixth period elements a comparison between the present and the X-ray data is not very significant, the accuracy of the X-ray data being too poor. The modified Moseley plot of the present data yields a much more regular curve than the corresponding plot for the $K$ energies in the fourth period. This indicates that the binding energies here are less sensitive to the crystal parameters. (It may be pointed out that the "chemical" shifts of the $K$ binding energies in the fourth period seem to be considerably more pronounced than the shifts of the $L_{III}$ energies in the fifth period. Cf. ref. [4] and [35].) A discontinuity in the modified Moseley diagram occurs between Au and Hg, while the elements on either side of this discontinuity fall on straight lines. From this we conclude that there may be considerable overlapping of the $5d$ and $6s$ bands as well as of the $6s$ and $6p$ bands. No quantitative theoretical treatment of the band structure of the heavy elements exists.

## ACKNOWLEDGEMENTS

My sincere thanks are due to Professor Kai Siegbahn, who initiated this investigation and whose continual interest has been a great source of encouragement. Further, I am indebted to Fil. lic. Carl Nordling for help with the measurements and for many valuable discussions. I also wish to thank Mr. William Parker, who showed much diligence and skill in helping with the source preparations and the electron microscopy. Finally, I am obliged to Fil. lic. Torsten Alväger of the Nobel Institute of Physics and Fil. mag. Bo Jung of the Werner Institute of Nuclear Chemistry for the mass separation of the Hg samples.

*Institute of Physics, University of Uppsala.*

## REFERENCES

1. Sandström, A. E., in Handbuch der Physik, XXX, 78, editor S. Flügge, Springer Verlag, Berlin (1955).
2. Richtmyer, F. K., Barnes, S. W., and Ramberg, E., Phys. Rev. *46*, 843 (1934).
3. Sokolowski, E., Nordling, C., and Siegbahn, K., Ark. Fys. *12*, 301 (1957).
4. Nordling, C., Sokolowski, E., and Siegbahn, K., Ark. Fys. *13*, 483 (1958).
5. Kittel, C., Introduction to Solid State Physics. Wiley and Sons, Inc., New York *14*, 557 (1956).
6. Siegbahn, K., and Edvarson, K., Nuc. Phys. *1*, 137 (1956).
7. Sokolowski, E., and Nordling, C., Ark. Fys. *14*, 557 (1959).
8. Hartree, D.R., Proc. Camb. Phil. Soc. *21*, 746 (1923).
9. Siegbahn, K., Ark. Mat. Astr. Fys., *30 A*, 1 (1944).
10. Du Mond, J. W. M., and Cohen, R. E., Rev. Mod. Phys. *25*, 691 (1953).
11. Gerholm, T. R., in Beta- and Gamma-Ray Spectroscopy, editor K. Siegbahn, North Holland Publishing Co., Amsterdam (1955).
12. Nordling, C., to be published in Ark. Fys. (1959).
13. Weisskopf, V., Phys. Zeitschr. *34*, 1 (1933).
14. Pines, D., in Solid State Physics, *1*, editors F. Seitz and D. Turnbull, Acad. Press Inc., New York (1955).
15. Lang, W., Optik *3*, 233 (1948).
    Kleinn, W., Optik *11*, 226 (1954).
16. Meyer, W., Zeitschr. Elektrochem. *50*, 274 (1944).
17. Beckman, O., private communication.
18. Ingelstam, E., Thesis, Nova Acta Reg. Soc. Sci. Upsal., *10* (1936).
19. Beckman, O., Axelsson, B., and Bergvall, P., to be published in Ark. Fys. (1959).
20. Zisman, W. A., Rev. Scient. Instr. *3*, 367 (1932).
21. Michaelson, H. B., Journ. Appl. Phys. *21*, 536 (1950).
22. Hagström, S., private communication.
23. Condon, E. U., and Shortley, H., The Theory of Atomic Spectra. Cambridge (1935).
24. Idei, S., Sci. Rep. Tôhoku Univ., *19*, 641 (1930).
25. Jones, H., and Mott, N. F., Proc. Roy. Soc. *A 162*, 49 (1937).
26. Krutter, H. M., Phys. Rev. *48*, 664 (1935).
27. Parratt, L. G., AFOSR TN-56-562, ASTIA AD 110 382, (ASTIA Document Service Center, Dayton 2, Ohio, U.S.A.) (1958).
28. Beeman, W. W., and Friedman, H., Phys. Rev. *56*, 392 (1939).
29. Sanner, V. H., Thesis, Univ. of Uppsala (1941).
30. Barnes, A. H., Phys. Rev. *44*, 141 (1933).
31. Howarth, D. J., Proc. Roy. Soc. (London) *A 220*, 513 (1953).
32. Slater, J. C., Phys. Rev. *49*, 537 (1936).
33. X-ray Diffraction Data, published by the American Society for Testing Materials.
34. Parratt, L. G., Hempstead, C. F. and Jossem, E. L., Phys. Rev. *105*, 1228 (1957).
35. Nordling, C., to be published in Ark. Fys. (1959).
36. Cauchois, Y., and Hulubei, C. R., Longeurs d'onde des émissions X et des discontinuité d'absorption X., Hermann, Paris (1947).

Tryckt den 19 januari 1959

Uppsala 1959. Almqvist & Wiksells Boktryckeri AB